Eur. Phys. J. Spec. Top. (2026) 235:8045–8053
https://doi.org/10.1140/epjs/s11734-026-02523-4

THE EUROPEAN PHYSICAL JOURNAL SPECIAL TOPICS

Regular Article

Higher-order triadic interactions in the EEG sensorimotor network during motor imagery

Vladimir Antipov[1,3,a], Semen Kurkin[1,3], and Susanna Gordleeva[2]

[1] Plekhanov Russian University of Economics, 36 Stremyanny Lane, Moscow, Russia
[2] Lobachevsky State University of Nizhny Novgorod, 23 Prospekt Gagarina (Gagarin Avenue), Nizhny Novgorod, Russia
[3] National Medical Research Center for Therapy and Preventive Medicine, 10 Petroverigskiy Pereulok, Moscow, Russia

Received 31 May 2026 / Accepted 7 July 2026 / Published online 22 July 2026
© The Author(s), under exclusive licence to EDP Sciences, Springer-Verlag GmbH Germany, part of Springer Nature 2026

Abstract Understanding how visual cues shape the network organisation underlying motor imagery remains a challenge. Whilst electroencephalography (EEG) studies typically focus on pairwise sensorimotor coupling, brain dynamics are increasingly understood through higher-order interactions. Here, we investigate this using the Triadic Interaction Mining framework, which identifies triads where one node modulates the interaction between two others. We hypothesise that visual context reorganises the network's higher-order regulatory structure rather than merely scaling sensorimotor activation. Applying this framework to EEG recordings of a healthy adult cohort, we assessed how μ-band power coupling between sensorimotor electrodes is modulated during motor imagery triggered by either a realistic hand image or an abstract dot. Our results reveal distinct patterns of triadic regulation. The abstract cue elicited dense regulation within frontoparietal and sensorimotor regions, where frontal sites repeatedly modulated edges terminating at the left parietal cortex. Conversely, the realistic cue yielded fewer triads, predominantly featuring occipital electrodes modulating sensorimotor coupling across both hemispheres. These findings suggest that the visual stimulus modifies the higher-order organisation of the motor imagery network, highlighting the influence of visual context on functional connectivity.

1 Introduction

Motor imagery is defined as the mental simulation of an action without overt movement. It is a widely studied paradigm in cognitive neuroscience and a core element of non-invasive brain–computer interfaces (BCIs) [1–3]. Its appeal comes from the fact that imagining a movement engages, to a large extent, the same sensorimotor circuits as actual execution, which makes it a natural model for studying motor cognition and a practical control signal for neurorehabilitation [4, 5]. Over more than two decades, electroencephalography (EEG) has provided a robust electrophysiological marker of motor imagery in the form of the μ-band desynchronisation over sensorimotor cortex [6, 7]. This phenomenon underlies most contemporary motor imagery BCIs and continues to inspire methodological developments aimed at improving the decoding of imagined movements from EEG [3, 8].

Age-related decline in motor control, including impaired posture, gait, and slowed movement execution, significantly reduces quality of life in older adults. Recent reviews have highlighted that advanced neurophysiological data analysis (such as spectral measures, complexity metrics, and functional connectivity) can reveal biomarkers of this decline and open avenues for targeted intervention strategies [9, 10]. Motor imagery, as a cognitively controlled task that engages sensorimotor circuits without overt movement, is particularly suitable for assessing such biomarkers and for designing brain–computer interface (BCI)-based neurorehabilitation protocols.

A factor that is often overlooked in classical motor imagery paradigms is the form of the visual cue that triggers the imagination. The same instruction to imagine a hand movement can be elicited by a realistic image of a hand or by an abstract symbol, and these two situations do not appear to engage the brain in the same way. When a body part is shown, the action observation network, which spans occipital, posterior parietal and premotor regions, is activated by the visual stimulus and provides a direct mapping between the observed effector and the corresponding motor representation [11, 12]. In contrast, when the cue is purely abstract, the imagined movement

[a] e-mail: vantipovm@gmail.com (corresponding author)

has to be generated internally from a more symbolic instruction, presumably with a stronger contribution of the frontoparietal control network [13, 14]. Recent EEG studies of visually guided motor imagery have begun to confirm that the form of the visual cue shapes the spatial distribution of functional connectivity during the task [15], yet most of these analyses remain at the level of pairwise coupling between channels or regions.

The pairwise view of brain connectivity, in which each pair of nodes is characterised by a scalar measure of statistical dependence, has been extremely productive, but it is increasingly recognised as incomplete [16, 17]. Many cognitive functions are supported by coordinated activity amongst several regions, and reducing such multi-way coordination to a collection of pairwise links discards information that is essential for understanding network organisation. This observation has motivated a rapid development of higher-order representations of brain networks, including hypergraphs constructed from EEG and magnetoencephalography (MEG) [18, 19] and information-theoretic decompositions that isolate genuine third-order dependencies in neural signals [20]. Higher-order descriptions have already revealed previously hidden organisational patterns in healthy development, attention and clinical populations [17, 21], suggesting that beyond-pairwise interactions are not a marginal correction to the pairwise picture but a structural feature of brain dynamics. The shift from pairwise to higher-order descriptions is part of a broader evolution of network analysis in neuroimaging, which has been systematically reviewed for fMRI data and shown to provide novel insights into both physiological and pathological brain states [22]. The integration of network science and artificial intelligence has substantially advanced the development of BCIs for medical applications, from the physical principles of neural signal decoding to large-scale rehabilitation systems for neurological and mental disorders [23, 24]. Moreover, network-based approaches have been used to map research trends in AI-driven medicine, highlighting the growing importance of functional connectivity and higher-order statistics in this domain [25].

Amongst the different forms of higher-order interaction, triadic interactions occupy a special place. A triadic interaction is the situation in which one node regulates, either positively or negatively, the strength of the interaction between two other nodes, and it cannot be reduced to a hyperedge or a simplex because the regulator does not participate as an equal partner in the interaction [26, 27]. This notion has a clear neurobiological motivation: glial cells modulate synaptic transmission between neurons, and analogous regulatory motifs exist at the network level whenever one region modulates the coupling of two others. A general algorithm for mining triadic interactions from data, the Triadic Interaction Mining (TRIM) framework, has been recently introduced and validated on synthetic dynamics and on gene expression data [27]. However, despite the importance of triadic motifs in neural systems, the application of this specific framework to human EEG, and particularly to motor imagery, remains largely unexplored.

Here, we close this gap by applying the TRIM framework to EEG recordings of healthy adults performing motor imagery under two visual conditions: a realistic hand image and an abstract dot. By assessing the conditional mutual information of μ-band power, we identify exploratory triads where a third electrode modulates the pairwise coupling between sensorimotor channels. To our knowledge, the application of this framework to human EEG remains largely unexplored, providing a novel information-theoretic window into how visual context shapes the network architecture of motor imagery.

2 Materials and methods

2.1 Experimental procedure

The experiment was designed to study the neurophysiological patterns of motor imagery under different visual stimulation conditions [3]. The general structure of the session is shown in Fig. 1A. It began with an oculomotor calibration, during which participants performed controlled eye movements (saccades, fixations, and blinks) on command. These recordings were later used to identify oculomotor activity by means of independent component analysis and to remove the corresponding artefacts from the EEG. A one-minute resting-state recording without any stimulus was then acquired and served as a baseline reference. The main block consisted of 60 motor imagery trials, and the session ended with a second one-minute resting-state recording identical to the first.

The trials were evenly distributed across four conditions defined by two stimulus types and two sides of the imagined movement. The stimulus was either a realistic image of a hand (left or right) or an abstract dot located to the left or to the right of the centre of the screen. When a hand was shown, participants imagined the movement of the corresponding hand; when a dot was shown, they imagined a movement of the left hand for a dot on the left and of the right hand for a dot on the right. The stimuli thus differed both in form, realistic versus abstract, and in the side of the target movement.

Each trial followed the same sequence, illustrated in Fig. 1B. First, a neutral background was displayed for 4 s. It was followed by a fixation cross whose duration was drawn at random from the interval between 1 and 1.5 s. The visual stimulus triggering motor imagery was then presented for 4 s. Finally, participants rated how well they had managed to imagine the movement on a visual analogue scale ranging from “poor” to “good”. The time allowed

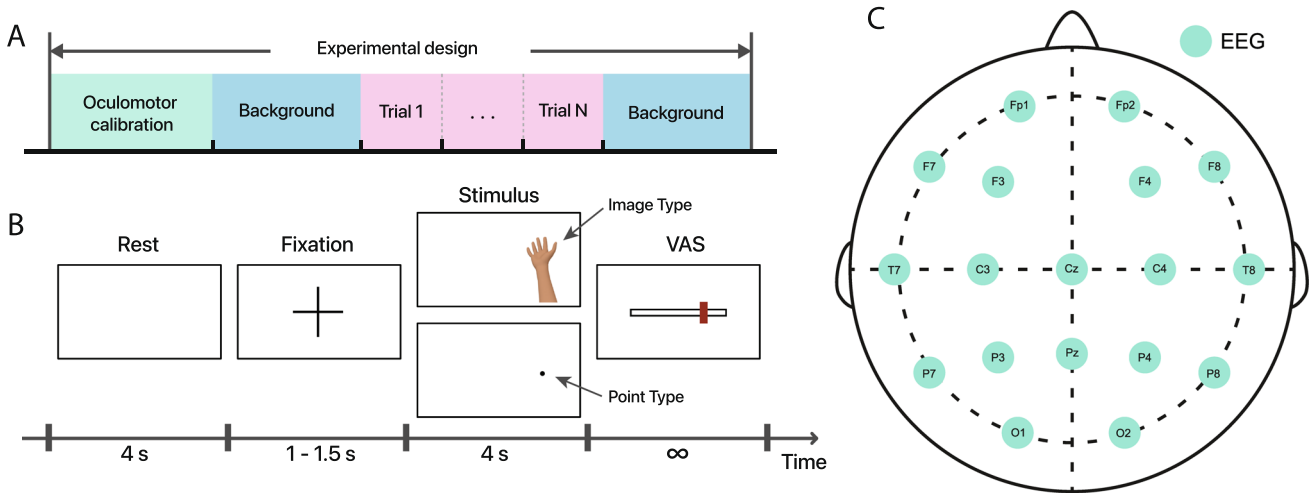


Fig. 1 Experimental design and EEG montage. (A) General structure of the experimental session, consisting of an oculomotor calibration, two background recordings, and a sequence of motor imagery trials. (B) Structure of a single trial: a rest interval (4 s) is followed by a fixation cross (1–1.5 s), a visual stimulus (4 s) triggering motor imagery, and a self-assessment phase on a visual analogue scale (VAS). The stimulus was either a realistic image of a hand (image type) or an abstract dot (point type). (C) Spatial arrangement of the 18 EEG electrodes used for analysis, positioned according to the international "10–20" system

for this self-assessment was not limited and lasted on average between 3 and 5 s. The VAS self-assessment was collected as part of the experimental design but lies outside the scope of the present analysis and is reserved for future work.

2.2 Participants

The study involved 24 healthy volunteers aged between 20 and 32 years (mean age = 25.3±3.4 years), none of whom had a history of neurological or psychiatric disorders. The experiment was approved by the Independent Ethics Committee of the Center for Clinical Research of the Immanuel Kant Baltic Federal University. All participants gave written informed consent prior to the experiment. The study was aimed at investigating the neurophysiological and subjective aspects of motor imagery, including the influence of the type of visual stimulus and of the subjective self-assessment on the strength of the corresponding patterns of brain activity.

2.3 Data acquisition and preprocessing

EEG signals were recorded using a NeoRec cap 21 system. Eighteen electrodes were selected for subsequent analysis according to the international "10–20" system. The reference and ground electrodes were placed at Fz and Fpz, respectively. EEG signals were recorded at a sampling rate of 500 Hz. The spatial arrangement of the electrodes on the scalp is shown in Fig. 1C.

EEG data preprocessing was performed using the MNE-Python library [28]. The recordings were resampled to an exact common sampling rate of 500 Hz: since the signals were streamed via the Lab Streaming Layer (LSL), whose effective sampling rate is not perfectly uniform owing to transmission latency and jitter, this step enforced a common and regular time base across recordings prior to analysis. The data were also re-referenced to the average of all electrodes. A finite impulse response (FIR) band-pass filter with a Hamming window (`firwin` design) was then applied in the 1–40 Hz range in order to remove low-frequency drifts and high-frequency noise prior to the decomposition. As visual inspection revealed no strongly contaminated channels, no bad-channel rejection or interpolation was applied, and all electrodes were retained. Ocular artefacts were subsequently removed using independent component analysis (ICA) [29], performed with the FastICA algorithm using 18 components. To this end, the oculomotor calibration recording, during which participants performed controlled saccades, fixations, and blinks on command, was used to identify the independent components associated with eye movements. These components were then excluded, and the clean EEG signals were reconstructed from the remaining components.

For the analysis, the continuous recordings were segmented into epochs spanning from 1.0 s before to 4.0 s after stimulus onset. This window captured both the fixation interval preceding the stimulus and the full duration of the motor imagery task. The pre-stimulus interval was later used as a baseline for normalising the spectral power, whilst only the 4 s of the motor imagery period entered the higher-order interaction analysis described below.

2.4 EEG higher-order triadic interactions

To detect higher-order triadic interactions, we adapted the TRIM framework [27] to the EEG recordings. The general principle is illustrated in Fig. 2: a triadic interaction occurs when one node Z, the regulator, modulates the strength of the interaction between two other nodes X and Y. In our setting, the nodes of the network correspond to the EEG electrodes, and the dynamical state of each node is given by the spectral power of its signal in the μ rhythm.

We focussed on the μ band (8–13 Hz), the sensorimotor analogue of the occipital alpha rhythm, whose desynchronisation is a well-established marker of motor imagery [6]. For each participant and condition, the single-trial band power was obtained as follows. A time-frequency representation of every epoch was computed with the multitaper method over the 4–30 Hz range, using a frequency-dependent number of cycles ($n_{\text{cycles}} = f/2$) corresponding to a constant analysis window of 0.5 s and a time-bandwidth product of 4.0, yielding three DPSS tapers, and the resulting power was normalised with respect to the pre-stimulus fixation interval. The normalised power was then restricted to the 4 s of the motor imagery period and averaged across the frequencies of the μ band and across time, yielding one power value per electrode and per trial. These single-trial values were averaged across the trials of each participant, so that every electrode was characterised by one μ-power value per participant and condition, and the values of each electrode were standardised across participants. In this way, and in contrast to the temporal time series used in the original formulation of the model, the role of the dynamical state of each node was played by the distribution of its μ power across the participant cohort.

Triadic interactions were searched for separately in the two stimulus conditions, Point and Image. As candidate edges X–Y, we considered all pairs formed by the nine electrodes overlying the sensorimotor and adjacent areas (F3, F4, C3, Cz, C4, T7, T8, P3, P4), giving $\binom{9}{2} = 36$ pairs. For each pair, every one of the remaining electrodes was tested as a candidate regulator Z.

For each candidate triad, the values of the regulator Z were sorted and partitioned into P bins defined by the quantiles of Z, so that each bin m_z contained the same number of observations and corresponded to a distinct range of values of Z. Within each bin, we estimated the mutual information between X and Y conditioned on that range of Z,

$$\mathrm{MI}_z(m) = \int dx \int dy\, \mu(x,\, y \mid z_m)\, \log\!\left[\frac{\mu(x,\, y \mid z_m)}{\mu(x \mid z_m)\, \mu(y \mid z_m)}\right], \tag{1}$$

where $\mu(x \mid z_m)$ and $\mu(y \mid z_m)$ are the marginal probability densities of X and Y in bin m_z, and $\mu(x,\, y \mid z_m)$ is their joint probability density. The quantity in Eq. (1) was estimated non-parametrically using k-nearest-neighbour entropy estimators [30]. Averaging $\mathrm{MI}_z(m)$ over the bins,

$$\langle \mathrm{MI}_z \rangle = \sum_{m=0}^{P-1} p(z_m)\, \mathrm{MI}_z(m), \qquad p(z_m) = \tfrac{1}{P}, \tag{2}$$

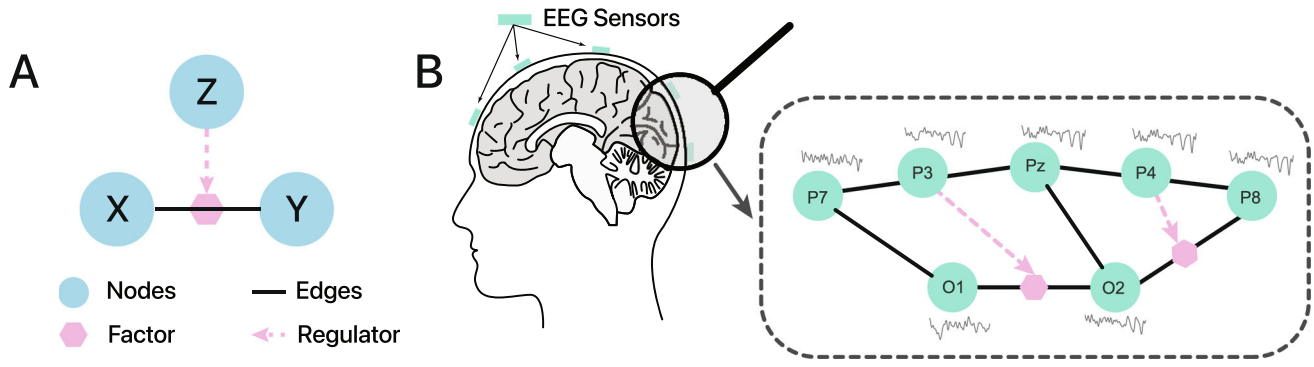


Fig. 2 Higher-order triadic interactions in EEG data. **A** Schematic of a triadic interaction: a regulator node Z modulates the strength of the interaction between two other nodes X and Y. The regulated edge is represented as a factor node (hexagon), and the regulatory link from Z is shown as a dashed arrow. **B** Application of the framework to EEG recordings: electrodes are treated as nodes whose dynamical state is given by the band power of their signal, structural edges connect pairs of nodes (solid lines), and candidate regulator nodes modulate these edges (dashed arrows)

recovers the conditional mutual information between X and Y given Z, where $p(z_m)$ is the probability that Z falls in bin m_z. As shown in Ref. [27], this average is by itself insensitive to the modulation of the interaction and is therefore not sufficient to reveal a triadic interaction.

The key observation is that a genuine triadic interaction manifests itself as a variation of $\mathrm{MI}_z(m)$ across the bins of Z, rather than in its mean. Following Ref. [27], we quantified this variation by the standard deviation of MI_z,

$$\Sigma = \sqrt{\sum_{m=0}^{P-1} p(z_m)\,[\,\mathrm{MI}_z(m) - \langle \mathrm{MI}_z \rangle\,]^2}. \tag{3}$$

A value of Σ close to zero indicates that $\mathrm{MI}_z(m)$ stays approximately constant, that is, the strength of the interaction between X and Y does not depend on Z, whereas a large Σ signals that Z modulates this interaction. The significance of the observed Σ was assessed against a randomisation null model obtained by shuffling the values of Z relative to those of X and Y, which disrupts any genuine triadic dependence whilst preserving the marginal distributions [31]. From 10^3 realisations of this null model, we computed the standardised score

$$\Theta_\Sigma = \frac{\Sigma - \mathbb{E}(\Sigma_{\mathrm{ran}})}{\sqrt{\mathbb{E}(\Sigma_{\mathrm{ran}}^2) - (\mathbb{E}(\Sigma_{\mathrm{ran}}))^2}}, \tag{4}$$

together with the empirical p-value

$$p_\Sigma = P(\Sigma_{\mathrm{ran}} > \Sigma), \tag{5}$$

where Σ_{ran} denotes the standard deviation of MI_z obtained on the surrogate data, and $\mathbb{E}(\cdot)$ the expectation over the null realisations. A triad was retained as a significant triadic interaction when $p_\Sigma < 0.05$. The retained triads were then ranked by Θ_Σ and displayed on the scalp, with the structural edge X–Y shown as a solid line and the regulatory link from Z as a dashed arrow pointing to the modulated edge.

3 Results

We applied the TRIM algorithm to the μ-band power of the 18 EEG electrodes, searching for triadic interactions separately in the 2 stimulus conditions. For each candidate edge connecting two sensorimotor electrodes, every remaining electrode was tested as a possible regulator. The triads reaching significance ($p_\Sigma < 0.05$) were retained and ranked by Θ_Σ. Across both conditions, 9 triads reached significance, 6 in the Point condition and 3 in the Image condition. The resulting interactions are displayed on the scalp in Fig. 3 for the Point (A) and Image (B) conditions.

The two conditions gave rise to clearly distinct patterns of triadic regulation. In the Point condition (Fig. 3A), the significant triads were more numerous and densely concentrated over the left central and parietal region, with the modulated edges repeatedly terminating at the parietal electrode P3 (four of the six edges, namely C3–P3, F3–P3, Cz–P3 and T8–P3). The strongest interaction of the whole analysis was found here, with the C3–P3 edge regulated by the frontal electrode F4 ($\Theta_\Sigma = 5.91$, $p_\Sigma = 0.007$), a value markedly above those of the remaining triads (Θ_Σ between 2.57 and 2.91, p_Σ between 0.024 and 0.034). The regulator nodes were located predominantly within the frontal and parieto-central areas themselves, with frontal sites acting as regulators in four of the six triads and F4 alone regulating two edges (C3–P3 and F3–P3). The regulation, therefore, took place largely inside the sensorimotor and frontoparietal system, indicating that during imagery driven by an abstract cue, the coupling between sensorimotor electrodes was modulated by other nodes of the same network.

In the Image condition (Fig. 3B), the picture was markedly sparser, with only three significant triads and a different organisation of the regulatory links. In all three, the regulator was an occipital electrode, O1 in two cases and O2 in one, and the modulated edges spanned both hemispheres, namely C3–P3 (regulated by O2, $\Theta_\Sigma = 2.99$, $p_\Sigma = 0.04$), T7–F3 (regulated by O1, $\Theta_\Sigma = 1.16$, $p_\Sigma = 0.04$) and T8–Cz (regulated by O1, $\Theta_\Sigma = 1.21$, $p_\Sigma = 0.04$). In other words, when the stimulus was a realistic image of a hand, the modulation of the sensorimotor coupling originated mainly from the visual electrodes, whereas the dense intra-sensorimotor regulation observed for the abstract stimulus was largely absent.

Taken together, these results show that the form of the visual stimulus reshapes the higher-order organisation of the sensorimotor network rather than simply changing the overall level of activity. The abstract Point cue was associated with a larger number of triads regulated within the frontoparietal and sensorimotor electrodes, whilst

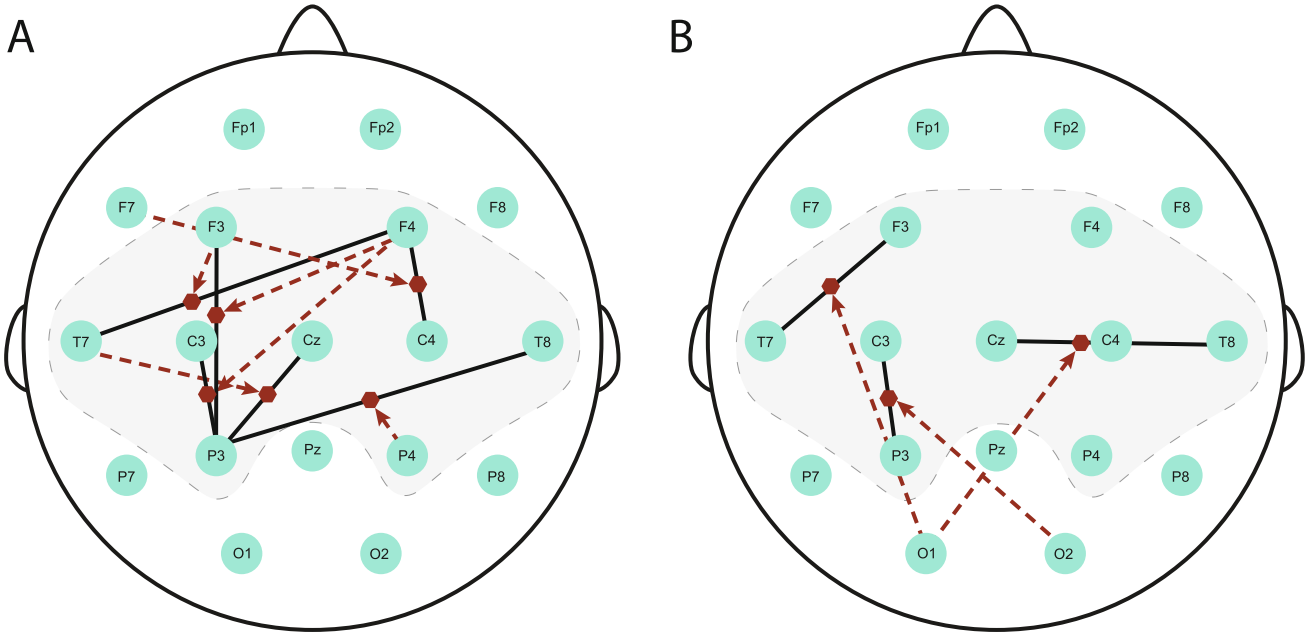


Fig. 3 Significant triadic interactions in the μ band identified by the TRIM algorithm for the Point **A** and Image **B** conditions. Each triadic interaction connects two end-point electrodes X and Y, joined by a solid structural edge, and a regulator electrode Z, whose modulatory link is shown as a dashed arrow pointing to the regulated edge (red hexagon). Only triads with $p_\Sigma < 0.05$ are displayed, and for each edge, the strongest interactions ranked by Θ_Σ are shown. The shaded area highlights the sensorimotor and adjacent electrodes used as candidate end-points of the regulated edges

the realistic Image cue was associated with fewer triads in which occipital electrodes regulated the sensorimotor coupling.

4 Discussion

In this study, we examined the higher-order organisation of the sensorimotor network during motor imagery under two visual stimulation conditions. Instead of restricting the analysis to pairwise coupling between EEG electrodes, we applied the TRIM framework [27] to the μ-band power of the electrodes, in order to identify triads in which the between-subject variation of the μ-power at a third electrode is associated with a reorganisation of the coupling between two sensorimotor electrodes. The main result is that the form of the visual stimulus reshaped the between-subject pattern of triadic statistical regulation amongst the EEG electrodes. The abstract Point cue was associated with a denser set of triads involving the frontoparietal and sensorimotor electrodes, whereas the realistic Image cue was associated with fewer triads in which the between-subject μ-power of occipital electrodes structured the sensorimotor coupling.

Our choice of the μ band is motivated by its established role as the sensorimotor analogue of the occipital alpha rhythm. The desynchronisation of the μ rhythm over sensorimotor cortex is one of the most robust electrophysiological markers of both movement and motor imagery [6, 7], and it has been repeatedly shown that imagery of hand movements engages the same sensorimotor generators as overt movement [4]. Working with μ-band power, therefore, allowed us to anchor the analysis in a frequency range that is directly relevant to the imagery task, whilst the triadic framework added a level of description that pairwise connectivity cannot reach. As emphasised by recent work on higher-order interactions in the brain, multivariate dependencies reveal aspects of network organisation that are systematically overlooked when only pairwise links are considered [16, 17], and triadic interactions in particular capture the situation in which one node regulates the relationship between two others rather than interacting with them directly [26, 27].

Crucially, because our analysis relies on participant-averaged data, the identified triads reflect between-subject statistical structures rather than direct intra-brain dynamics. We, therefore, use terms like “regulator” as shorthand, offering the underlying neurophysiological mechanism as a working hypothesis for future within-subject validation. The pattern observed for the realistic hand image is compatible with the involvement of the action observation network. When a body part is shown, the lateral occipitotemporal and parietal regions of this network translate the observed effector into the corresponding motor representation, forming a bidirectional circuit between

visual and motor areas [11, 12]. In our data, this is reflected by the between-subject μ-power of the occipital electrodes O1 and O2 co-varying with the coupling of the sensorimotor edges, which we tentatively interpret as a statistical footprint of the visual representation of the hand shaping the coupling within the motor system across the cohort. The relatively small number of triads in this condition is compatible with the idea that a realistic effector provides a concrete visual template, so that the mapping from vision to motor representation is comparatively direct and does not require extensive regulation distributed across the motor network.

The abstract Point cue produced a different picture. Here the between-subject regulation was concentrated within the frontal, central and parietal electrodes themselves, with the μ-power at frontal sites co-varying with the coupling of several sensorimotor edges. This is in line with evidence that motor imagery is supported by a distributed frontoparietal network, in which premotor and posterior parietal regions interact to construct and maintain the mental simulation of movement [13, 14]. When the stimulus does not contain a body part, the imagined movement cannot be read out directly from the visual input and has to be generated internally from a more symbolic cue. Our results suggest that this internally driven construction is accompanied at the cohort level by a richer set of triadic interactions within the frontoparietal and sensorimotor electrodes, a pattern compatible with a greater reliance on top-down control when the stimulus is abstract [5, 14]. The contrast between the two conditions, thus, indicates that the difference between realistic and abstract cues is not merely a change in the overall level of sensorimotor activation, but a reorganisation of which electrodes statistically modulate the coupling within the motor system.

From a translational perspective, understanding how the form of a visual cue reshapes higher-order regulatory structures can inform the design of more effective BCI-based neurorehabilitation protocols. For instance, vibrotactile neurofeedback training has been shown to improve motor cortical excitability during motor imagery [32], and functional near-infrared spectroscopy (fNIRS) can classify motor-related brain activity at the sensor level, offering a portable alternative to EEG [33]. Furthermore, transcranial magnetic stimulation (TMS) of the dorsolateral prefrontal cortex has been found to increase posterior theta rhythm and reduce motor imagery latency, demonstrating that non-invasive neuromodulation can alter the temporal dynamics of the imagery network [34]. The triadic interactions identified here provide a candidate mechanistic link between such external interventions and the reorganisation of sensorimotor coupling: each of these techniques may exert its effect by selectively modulating the regulatory influence of a specific node (e.g. a frontal or occipital electrode) on distal sensorimotor edges.

These findings also connect to a growing body of work that applies higher-order and information-theoretic tools to neural data. Triadic and other beyond-pairwise descriptions have recently been used to characterise the multiscale organisation of brain networks in development and in clinical populations [21], and information-geometric decompositions have been used to extract genuine third-order interactions from EEG during imagined movements [20]. Our work adds to this literature by showing that the specific notion of a regulated edge, in which between-subject variations in the activity of one electrode are associated with the coupling between two others, can be mined from EEG and is sensitive to the experimental condition. This opens the way to use the triadic framework as a complementary description of task-related brain network reorganisation.

4.1 Limitations

Several limitations should be kept in mind when interpreting these results. First, the dynamical variable used for each electrode was its participant-averaged μ-band power. Consequently, the analysis captures inter-individual network differences across the cohort rather than intra-individual temporal dynamics, offering a cross-sectional perspective on sensorimotor state variability. Whilst our results capture task-related network reorganisation at the between-subject level, mapping these statistical dependencies onto real-time physiological mechanisms remains a direction for future within-subject research. Second, significance was assessed with the randomisation null model and the threshold $p_\Sigma < 0.05$, without correction for the number of tested triads; the reported interactions are therefore intended to generate hypotheses that should be confirmed on independent and larger samples, ideally complemented by the Gaussian null model and the entropic score that are part of the full TRIM pipeline [27]. As reviewed recently for fMRI networks, the transition from pairwise to higher-order descriptions requires careful validation against null models and, ideally, independent replication cohorts [22]. Third, the analysis was carried out at the sensor level, so that the anatomical interpretation of the involved electrodes remains tentative and would benefit from source reconstruction. Finally, the present analysis pooled the two sides of the imagined movement and focussed on the contrast between realistic and abstract stimuli; the lateralisation of the triadic interactions and their dependence on the imagined hand are natural directions for future work.

5 Conclusion

Our study demonstrates that the form of the visual cue used to trigger motor imagery is associated with a reorganisation of the between-subject pattern of triadic statistical regulation amongst EEG electrodes, rather than

simply scaling the overall level of sensorimotor activation. Using the TRIM framework applied to the μ-band power of EEG recordings, we identified triads in which between-subject variations in the μ-power of a third electrode co-vary with the coupling between two sensorimotor electrodes, and we found markedly distinct patterns across the two conditions. The abstract dot was associated with denser triads within the frontoparietal and sensorimotor electrodes, with the μ-power at frontal sites repeatedly co-varying with the strength of edges terminating at left parietal cortex, a pattern compatible with a stronger reliance on internally generated, top-down control of the imagined movement. In contrast, the realistic hand image was associated with fewer triads in which the μ-power of occipital electrodes structured sensorimotor coupling across both hemispheres, a pattern compatible with the engagement of the action observation network when a body part is visually available as a template. Whilst this cross-sectional analysis primarily characterises the network's architecture at the cohort level, these findings clearly indicate that beyond-pairwise descriptions of EEG connectivity carry information that pairwise measures cannot reach, and they open the way to using the triadic interaction framework as a complementary tool for studying task-related reorganisation of brain networks in motor imagery and beyond.

Acknowledgements The work was funded by the Russian Science Foundation (Grant No. 25-69-00047, https://rscf.ru/project/25-69-00047/).

Data Availability The data presented in this study are available on request from the corresponding author.

References

1. R. Mane, T. Chouhan, C. Guan, Bci for stroke rehabilitation: motor and beyond. J. Neural Eng. **17**(4), 041001 (2020). https://doi.org/10.1088/1741-2552/aba162
2. O. Drapkina, A. Savosenkov, S. Gordleeva, S. Kurkin, A. Badarin, N. Grigorev et al., Characteristics of the specific brain functional network correlate with the latency of motor imagery. The European Physical Journal Special Topics **233**(3), 479–488 (2024)
3. A.A. Badarin, V.M. Antipov, O.M. Drapkina, A.R. Kiselev, Spatiotemporal dynamics of functional connectivity networks in eeg-based motor imagery. Russian Open Medical Journal **14**(4), 423 (2025)
4. G. Pfurtscheller, C. Neuper, Motor imagery activates primary sensorimotor area in humans. Neurosci. Lett. **239**(2–3), 65–68 (1997)
5. M. Mustile, D. Kourtis, M.G. Edwards, D.I. Donaldson, M. Ietswaart, Neural correlates of motor imagery and execution in real-world dynamic behavior: evidence for similarities and differences. Front. Hum. Neurosci. **18**, 1412307 (2024)
6. G. Pfurtscheller, F.L. Da Silva, Event-related eeg/meg synchronization and desynchronization: basic principles. Clin. Neurophysiol. **110**(11), 1842–1857 (1999)
7. D.J. McFarland, L.A. Miner, T.M. Vaughan, J.R. Wolpaw, Mu and beta rhythm topographies during motor imagery and actual movements. Brain Topogr. **12**(3), 177–186 (2000)
8. S. Chen, M. Chen, X. Wang, X. Liu, B. Liu, D. Ming, Brain-computer interfaces in 2023–2024. Brain-x **3**(1), e70024 (2025)
9. S. Gordleeva, N. Grigorev, E. Pitsik, S. Kurkin, V. Kazantsev, A. Hramov, Detection and rehabilitation of age-related motor skills impairment: Neurophysiological biomarkers and perspectives. Ageing Res. Rev. **113**, 102923 (2026). https://doi.org/10.1016/j.arr.2025.102923
10. N.S. Frolov, E.N. Pitsik, V.A. Maksimenko, V.V. Grubov, A.R. Kiselev, Z. Wang et al., Age-related slowing down in the motor initiation in elderly adults. PLoS ONE **15**(9), e0233942 (2020). https://doi.org/10.1371/journal.pone.0233942
11. G. Vannuscorps, F. Wurm, M, Striem-Amit E, Caramazza A, Large-scale organization of the hand action observation network in individuals born without hands. Cereb. Cortex **29**(8), 3434–3444 (2019)
12. A. Eroğlu, B.A. Urgen, Top-down modulation of visual action perception: distinct task effects in the action observation network. Brain Struct. Funct. **230**(9), 175 (2025)
13. S. Pilgramm, B. de Haas, F. Helm, K. Zentgraf, R. Stark, J. Munzert et al., Motor imagery of hand actions: Decoding the content of motor imagery from brain activity in frontal and parietal motor areas. Hum. Brain Mapp. **37**(1), 81–93 (2016)
14. L. Chen, L. Zhang, Z. Wang, Q. Li, B. Gu, D. Ming, Task-related reconfiguration patterns of frontoparietal network during motor imagery. Neuroscience **579**, 302–311 (2025). https://doi.org/10.1016/j.neuroscience.2025.05.035
15. T. Wang, Y.H. Chen, M. Sawan, Exploring the role of visual guidance in motor imagery-based brain-computer interface: An eeg microstate-specific functional connectivity study. Bioengineering **10**(3), 281 (2023)
16. F. Battiston, G. Cencetti, I. Iacopini, V. Latora, M. Lucas, A. Patania et al., Networks beyond pairwise interactions: Structure and dynamics. Phys. Rep. **874**, 1–92 (2020)
17. F. Santos, P. Tewarie, P. Baudot, A. Luchicchi, D. Barros de Souza, G. Girier et al., (2023) Emergence of high-order functional hubs in the human brain. bioRxiv https://doi.org/10.1101/2023.02.10.528083
18. N. Peña Serrano, R. Jaimes-Reátegui, A.N. Pisarchik, Hypergraph of functional connectivity based on event-related coherence: Magnetoencephalography data analysis. Appl. Sci. **14**(6), 2343 (2024)

19. A.N. Pisarchik, N. Peña Serrano, E. Puente, W. de la Vega, R. Jaimes-Reátegui, Hypergraph analysis of functional brain connectivity during figurative attention. Appl. Sci. **15**(7), 3833 (2025)
20. E. Albers, P. Marriott, M. Tatsuno, Using information geometry to characterize higher-order interactions in eeg (2025), arXiv preprint arXiv:2510.14188
21. Q. Li, S. Yu, J. Malo, G.D. Pearlson, Y.P. Wang, V.D. Calhoun, Higher-order triadic interactions: Insights into the multiscale network organization in schizophrenia. Hum. Brain Mapp. **46**(16), e70399 (2025)
22. S. Kurkin, A. Pisarchik, L. Mayorova, A. Hramov, Evolution of methods for assessing fmri-based functional networks: From classical pairwise connectivity to higher-order interactions. Phys. Rep. **1174**, 1–66 (2026). https://doi.org/10.1016/j.physrep.2026.02.004
23. A. Hramov, V. Maksimenko, A. Pisarchik, Physical principles of brain-computer interfaces and their applications for rehabilitation, robotics and control of human brain states. Phys. Rep. **918**, 1–133 (2021). https://doi.org/10.1016/j.physrep.2021.03.002
24. V. Khorev, S. Kurkin, A. Badarin, V. Antipov, E. Pitsik, A. Andreev et al., Review on the use of brain computer interface rehabilitation methods for treating mental and neurological conditions. J. Integr. Neurosci. **23**(7), 125 (2024). https://doi.org/10.31083/j.jin2307125
25. O. Karpov, E. Pitsik, S. Kurkin, V. Maksimenko, A. Gusev et al., Analysis of publication activity and research trends in the field of ai medical applications: Network approach. Int. J. Environ. Res. Public Health **20**(7), 5335 (2023). https://doi.org/10.3390/ijerph20075335
26. A.P. Millán, H. Sun, J.J. Torres, G. Bianconi, Triadic percolation induces dynamical topological patterns in higher-order networks. PNAS nexus **3**(7), 270 (2024)
27. M. Niedostatek, A. Baptista, J. Yamamoto, J. Kurths, R. Sanchez Garcia, B.D. MacArthur et al., Mining higher-order triadic interactions. Nat. Commun. **16**(1), 11613 (2025). https://doi.org/10.1038/s41467-025-66577-z
28. A. Gramfort, M. Luessi, E. Larson, D.A. Engemann, D. Strohmeier, C. Brodbeck et al., Meg and eeg data analysis with mne-python. Front. Neuroinform. **7**, 267 (2013)
29. J. Iriarte, E. Urrestarazu, M. Valencia, M. Alegre, A. Malanda, C. Viteri et al., Independent component analysis as a tool to eliminate artifacts in eeg: a quantitative study. J. Clin. Neurophysiol. **20**(4), 249–257 (2003)
30. A. Kraskov, H. Stögbauer, P. Grassberger, Estimating mutual information. Phys. Rev. E **69**, 066138 (2004). https://doi.org/10.1103/PhysRevE.69.066138https://link.aps.org/doi/10.1103/PhysRevE.69.066138
31. J. Theiler, S. Eubank, A. Longtin, B. Galdrikian, J.D. Farmer, Testing for nonlinearity in time series: the method of surrogate data. Physica D **58**(1–4), 77–94 (1992)
32. N. Grigorev, A. Savosenkov, M. Lukoyanov, A. Udoratina et al., A bci-based vibrotactile neurofeedback training improves motor cortical excitability during motor imagery. IEEE Trans. Neural Syst. Rehabil. Eng. **29**, 1583–1592 (2021). https://doi.org/10.1109/TNSRE.2021.3097438
33. A. Hramov, V. Grubov, A. Badarin, V. Maksimenko, A. Pisarchik, Functional near-infrared spectroscopy for the classification of motor-related brain activity on the sensor-level. Sensors **20**(8), 2362 (2020). https://doi.org/10.3390/s20082362
34. S. Kurkin, S. Gordleeva, A. Savosenkov, N. Grigorev, N. Smirnov, V. Grubov et al., Transcranial magnetic stimulation of the dorsolateral prefrontal cortex increases posterior theta rhythm and reduces latency of motor imagery. Sensors **23**(10), 4661 (2023). https://doi.org/10.3390/s23104661

Springer Nature or its licensor (e.g. a society or other partner) holds exclusive rights to this article under a publishing agreement with the author(s) or other rightsholder(s); author self-archiving of the accepted manuscript version of this article is solely governed by the terms of such publishing agreement and applicable law.